Comparison of OTFS Diversity Performance over Slow and Fast Fading Channels

Hongyang Zhang, Xiaojing Huang, and J. Andrew Zhang

University of Technology Sydney, Ultimo, NSW, 2007, Australia
Emails: Hongyang.ZHANG-1@student.uts.edu.au
{Xiaojing.Huang,Andrew.Zhang}@uts.edu.au

***Abstract*—Orthogonal time frequency space (OTFS) modulation shows great performance improvement over high-mobility wireless channels compared with traditional orthogonal frequency division multiplexing (OFDM). In this paper, we first derive the input and output relationship of OTFS signal in the delay-time domain, which shows that OTFS can be regarded as a combination of OFDM and single-carrier frequency-division multiple access (SC-FDMA). We then examine the diversity order of an OTFS system through received signal-to-noise ratio analysis and predict that this modulation technique can potentially achieve full diversity in both delay and Doppler domains. Finally, we simulate the OTFS performance based on 5G tapped-delay-line channel models under both slow and fast fading conditions. Extensive simulation results confirm that OTFS performs significantly better than other modulation techniques in fast fading channels.**

***Index Terms*—OTFS, OFDM, single-carrier, diversity, delay-Doppler channel**

I. Introduction

Orthogonal time frequency space (OTFS) modulation is promising for next generation wireless communication systems with high-mobility applications. By mapping the transmitted signal into the delay-Doppler domain [1], the adverse effects of the high-mobility environment can be significantly reduced. When a channel is slow fading and frequency selective, traditional modulation and coding methods, such as orthogonal frequency division multiplexing (OFDM), transmit the signal over a set of parallel frequency channels. Although OFDM offers high spectral efficiency and low-complexity equalization, it does not perform well in high-Doppler scenarios, such as vehicle-to-vehicle communications and data transmissions from base stations to high-speed trains. When channel fading is fast with large Doppler frequency shift, OTFS exploits both time and frequency diversity, providing a significant improvement over OFDM by combating the Doppler effect.

OTFS was evolved from OFDM and there are strong research interests in connecting them. In [2], it was shown that OTFS outperforms OFDM in sub 6 GHz channels which were simulated by a ray launching method. Variations of OTFS have been developed by referring to OFDM. In [3], the Heisenberg transform in the OTFS modulation is replaced by OFDM modulation with cyclic prefix (CP) being added in every row of data symbol matrix. Compared to the original OTFS modulation, the computational complexity is reduced. In [4], such OFDM-based OTFS is applied in multiple-input and multiple-output (MIMO) system. In [5], by analyzing the input and output relationship in vector form, greater benefits can be achieved for practical OTFS receiver design and different pulse-shaping waveforms are taken into consideration. Meanwhile, the OTFS signal model is generalized based on general orthonormal basis functions in [6]. A multiple-access (MA) method is proposed for the uplink OTFS system in [7] to avoid multi-user interference.

Signal detection techniques are critical for the performance of OTFS systems. A Markov chain Monte Carlo (MCMC) sampling based low-complexity OTFS signal detection and a PN pilot sequence based channel estimation scheme are proposed in [8]. A novel low-complexity efficient message passing (MP) algorithm is developed to improve the bit-error-rate (BER) performance in [9] and [10]. This MP algorithm has also been generalized to asymmetric orthogonal frequency division multiplexing (A-OFDM) in [11]. Other MIMO-OTFS systems are also studied in [12].

Although the above mentioned researches on OTFS demonstrate significant improvement in BER performance over OFDM, most of the analyses and simulations were not performed based on practical system or channel model. Power delay profiles are mostly set as uniform distribution and only Rayleigh fading is considered in the transmission channels. Filling in this gap, this paper compares the performance of OTFS with OFDM using recently developed 5G channel models [13]. These are originally slow fading channels with time delay and power profiles set differently for different scenarios. We extend them to fast fading models by considering Doppler shift. Given the maximum movement speed, we can determine the maximum Doppler shift. Hence fast fading channels can be modeled by adding random Doppler shifts to all taps, which obey a uniform distribution within the Doppler spread.

The rest of this paper is organized as follows. Section II introduces the OTFS signal and system models. In Section III, we represent the received OTFS signal in matrix form in the delay-time domain and predict that OTFS can achieve full time and frequency diversity. In Section IV, we apply the 5G channel models to simulate OTFS in different scenarios under different channel conditions and compare it with other modulations. Finally, conclusions are drawn in Section V.

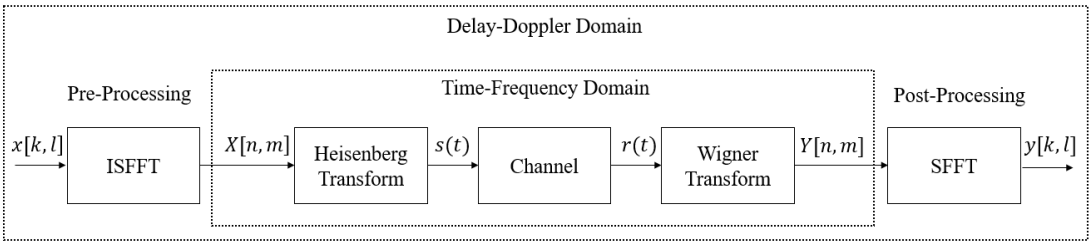

Fig. 1. OTFS modulation/demodulation scheme.

II. Signal and System Models

We consider a single input single output (SISO) OTFS system which transmits and receives uncoded quadrature-amplitude-modulation (QAM) symbols. It can be seen as a scheme that adds pre- and post-processing modules to a traditional OFDM system. The OTFS modulation/demodulation process is shown in Fig. 1. Firstly, at the transmitter, the QAM symbols are arranged in a two dimensional (2-D) matrix with N columns in the Doppler domain and M rows in the delay domain. Then the signal is transformed into the time-frequency domain through the inverse symplectic finite Fourier transform (ISFFT). After the Heisenberg transform, the signal is converted into time domain and passed through the double-dispersive channel. At the receiver, the received signal is processed by Wigner Transform and SFFT.

The time-frequency grid is discretized into resolutions of T and Δf with a set of time-frequency elements

$$\Phi = \{(kT, l\Delta f), k = 0, ..., N-1, l = 0, ..., M-1\}, \quad (1)$$

where T is the time duration of M QAM symbols and Δf is the subcarrier frequency spacing. After the ISFFT processing, the time-frequency domain signal can be expressed as

$$X[n, m] = \frac{1}{\sqrt{NM}} \sum_{k=0}^{N-1} \sum_{l=0}^{M-1} x[k, l] e^{j2\pi\left(\frac{nk}{N} - \frac{ml}{M}\right)}, \quad (2)$$

where $x[k, l]$ is the delay-Doppler domain signal and the delay-Doppler grid is defined as the set

$$\Psi = \left\{ \left(\frac{n}{NT}, \frac{m}{M\Delta f} \right), n = 0, ..., N-1, m = 0, ..., M-1 \right\}, \quad (3)$$

where $f_r = 1/NT$ and $d_r = 1/M\Delta f$ are the Doppler resolution and delay resolution respectively.

After reshaping the matrix $X[n, m]$ into time domain sequence, the Heisenberg transform [1] [14] is used to generate the time domain signal

$$s(t) = \sum_{n=0}^{N-1} \sum_{m=0}^{M-1} X[n, m] g_{tx}(t - nT) e^{j2\pi m\Delta f(t-nT)}, \quad (4)$$

where $g_{tx}(t)$ is the window function. Then $s(t)$ is transmitted through the delay-Doppler channel, and the received signal can be expressed as

$$r(t) = \int \int h(\tau, \nu) s(t - \tau) e^{j2\pi\nu t} d\tau d\nu + w(t), \quad (5)$$

where $h(\tau, \nu)$ is the channel delay-Doppler response and $w(t)$ is the additive white Gaussian noise. For a sparse P path channel, $h(\tau, \nu)$ is defined as

$$h(\tau, \nu) = \sum_{i=1}^{p} h_i \delta(\tau - \tau_i)\delta(\nu - \nu_i), \quad (6)$$

where h_i, τ_i, and ν_i are the path gain, delay and Doppler shift of the i th path respectively. Further defining the channel delay-time response as

$$h_t(\tau, t) = \int h(\tau, \nu) e^{j2\pi\nu t} d\nu, \quad (7)$$

the received signal can be expressed as

$$\begin{aligned} r(t) &= \int h_t(\tau, t) s(t - \tau) d\tau + w(t) \\ &= \int h_t(t - \tau, t) s(\tau) d\tau + w(t). \end{aligned} \quad (8)$$

At the receiver, there will be a Wigner transform to firstly map the received signal from the time domain to the time-frequency domain. The Wigner transform is defined as

$$Y[n, m] = [\int g_{rx}(t - \tau) r(t) e^{-j2\pi\nu(t-\tau)} dt]|_{\tau=nT, \nu=m\Delta f}, \quad (9)$$

where $g_{rx}(t)$ is the window function. Then, the signal is decoded by SFFT as

$$y[k, l] = \frac{1}{\sqrt{NM}} \sum_{n=0}^{N-1} \sum_{m=0}^{M-1} Y[n, m] e^{-j2\pi\left(\frac{nk}{N} - \frac{ml}{M}\right)}. \quad (10)$$

Because of Doppler effects and delay spread of the channel, equalization has to be applied to recover data symbols from $y[k, l]$. Most of the recent equalization algorithms are based on maximum likelihood estimation (MLE) and maximum A Posteriori (MAP) estimation. Message passing and MCMC have also been shown to produce relatively good performance in recovering data symbols. In this paper, we choose to use the minimum mean squared error (MMSE) equalization technique which also performs well compared with the methods mentioned above, with the advantage of lower complexity.

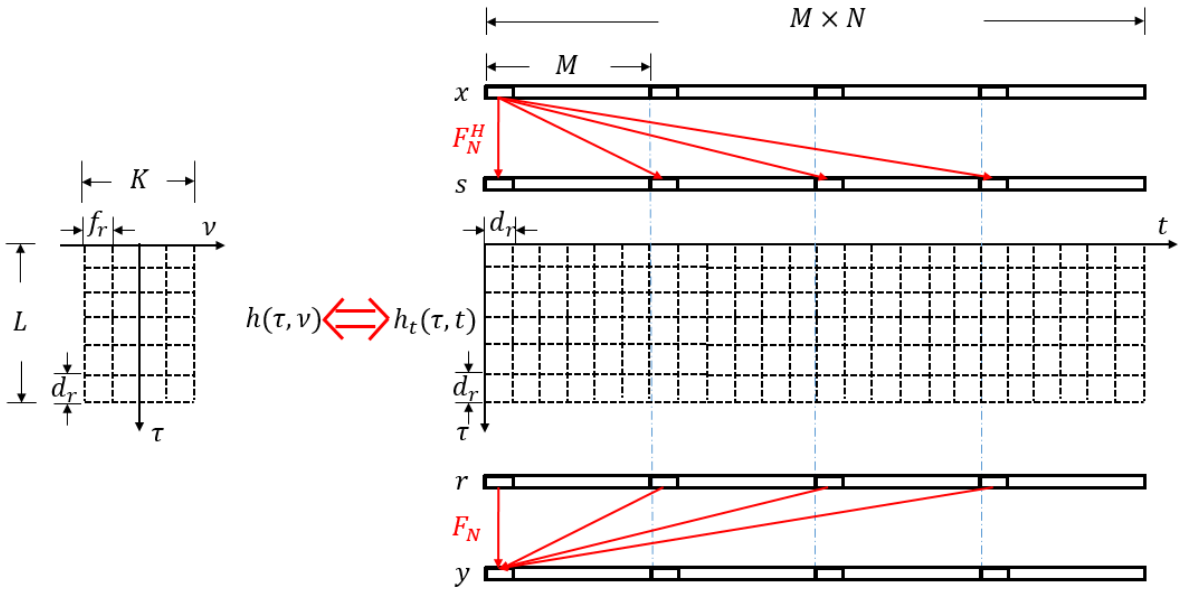

Fig. 2. OTFS signal transforms before and after channel with delay-time response.

III. Diversity Analysis

In a slow fading multipath channel, OTFS shows the characteristics of both traditional OFDM and SC-FDMA [11]. It balances the spectral efficiency and peak-to-average power ratio (PAPR) and demonstrates great BER performance.

To analyze the OTFS system in fast fading channels, we rewrite the formulas in Section II into vectors and matrices. We use $\otimes$ to denote Kronecker product and $vec(\cdot)$ to denote the vectorization that converts an $M \times N$ matrix to an $MN \times 1$ vector. Let $\mathbf{x} = vec(\mathbf{D})$ denote the signal to be transmitted where $\mathbf{D} \in C^{M \times N}$ is the 2-D data matrix. At the transmitter, the ISFFT operation can be written as

$$\mathbf{X} = \mathbf{F}_M \mathbf{D} \mathbf{F}_N^H, \tag{11}$$

where $\mathbf{X} \in C^{M \times N}$ is the signal to be sent in the time-frequency domain, $\mathbf{F}_M$ and $\mathbf{F}_N^H$ are the FFT and IFFT matrices respectively. From (4), the Heisenberg transform is expressed as

$$\mathbf{S} = \mathbf{G}_{tx} \mathbf{F}_M^H \mathbf{X} = \mathbf{G}_{tx} \mathbf{F}_M^H (\mathbf{F}_M \mathbf{D} \mathbf{F}_N^H) = \mathbf{G}_{tx} \mathbf{D} \mathbf{F}_N^H. \tag{12}$$

The matrix $\mathbf{S}$ is then converted into the time domain in vector form

$$\mathbf{s} = vec(\mathbf{S}) = (\mathbf{F}_N^H \otimes \mathbf{G}_{tx})\mathbf{x}. \tag{13}$$

Assuming that the channel memory length is L, we add a CP of length $(L-1)$ to the signal. The received signal after the delay-Doppler channel can be written as

$$\mathbf{r} = \mathbf{H}\mathbf{s} + \mathbf{w}, \tag{14}$$

where $\mathbf{H}$ is defined as

$$\mathbf{H} = \begin{bmatrix} h_t(0,0) & \cdots & h_t(2d_r,0) & h_t(d_r,0) \\ h_t(d_r,d_r) & \cdots & h_t(3d_r,d_r) & h_t(2d_r,d_r) \\ \vdots & \ddots & \ddots & \vdots \\ 0 & \cdots & \cdots & h_t(0,(MN-1)d_r) \end{bmatrix}. \tag{15}$$

The received baseband signal then goes through pulse shaping, Wigner transform and SFFT processing modules. Reformating $\mathbf{r}$ as an $M \times N$ matrix $\mathbf{R}$, the output signal from these modules can be obtained as

$$\mathbf{Y} = \mathbf{F}_M^H (\mathbf{F}_M \mathbf{G}_{rx} \mathbf{R}) \mathbf{F}_N. \tag{16}$$

Finally, the signal is reshaped into vector form

$$\mathbf{y} = (\mathbf{F}_N \otimes \mathbf{G}_{rx})\mathbf{r}, \tag{17}$$

where $\mathbf{G}_{rx}$ is the shaping pulse at the receiver. We assume that the OTFS system uses typical rectangular pulse shaping, where the pulse shaping matrix $\mathbf{G}_{tx}$ and $\mathbf{G}_{rx}$ are identity matrices. Hence, the input-output relationship of OTFS signal is expressed as

$$\mathbf{y} = (\mathbf{F}_N \otimes \mathbf{I}_M)\mathbf{H}(\mathbf{F}_N^H \otimes \mathbf{I}_M)\mathbf{x} + (\mathbf{F}_N \otimes \mathbf{I}_M)\mathbf{w}. \tag{18}$$

Further analysis shows that, except for a scaling factor, the received signal-to-noise ratio can be expressed as

$$\gamma \propto \sum_{l=0}^{L-1} \sum_{k=-[\frac{K}{2}]+1}^{[\frac{K}{2}]} |h(ld_r, kf_r)|^2 \cdot \frac{\sigma_s^2}{\sigma_w^2}, \text{ for even } K, \tag{19}$$

or

$$\gamma \propto \sum_{l=0}^{L-1} \sum_{k=-[\frac{K}{2}]}^{[\frac{K}{2}]} |h(ld_r, kf_r)|^2 \cdot \frac{\sigma_s^2}{\sigma_w^2}, \text{ for odd } K, \qquad (20)$$

where σ_s^2 is the transmitted signal power, σ_w^2 is the noise power, K is the total number of resolvable Doppler shifts and $[x]$ denotes the operation of taking the integer part of x.

From (12) and (13), we see that OTFS applies N-point FFTs on data symbols which are spaced M-symbol apart in an SC-FDMA modulated signal $\mathbf{x}$. The original signal $\mathbf{x}$ consists of N sections, each consisting of M data symbols. As depicted in Fig. 2, the N-point FFT spreads a data symbol in $\mathbf{x}$ to every section of $\mathbf{s}$. In this way, a data symbol can experience different time variations due to Doppler shift through the channel. After the received signal $\mathbf{r}$ is converted to $\mathbf{y}$, a received signal can achieve the time diversity provided by the fast fading channel. From [15], we know that, for SC-FDMA with the number of multipath L, if the desired spectral efficiency and the transmission block length is well controlled, a full diversity of order L is achievable. Moreover, it is shown that MMSE is able to achieve diversity order from 1 to L, while zero-forcing (ZF) equalization always achieves diversity order 1.

OTFS shows similar characteristics to SC-FDMA if $M \geqslant L$ so that it is able to achieve full frequency diversity. Similarly, given the number of Doppler shifts $K \leqslant N$, full time diversity of order K can be exploited in Doppler domain due to the N-point FFT. Therefore, OTFS can achieve full diversity in delay-Doppler domain with diversity order $K \times L$.

IV. Simulation Results

The tapped delay line (TDL) models are adopted to evaluate the performance of OTFS in an SISO transmitter and receiver setup. Based on TR 38 901 [13], three TDL models, namely TDL-A, TDL-B and TDL-C, are constructed to represent three different channel profiles for non-line-of-sight (NLOS) conditions while TDL-D and TDL-E are constructed for line-of-sight (LOS) conditions. Meanwhile, four different scenarios including UMi Street-canyon, UMa, RMa and UMi/Uma O2I are also defined, which determine the delay spread in taps.

In this section, we simulate three modulation methods including traditional OFDM, SC-FDMA and OTFS. The systems are tested under different scenarios, LOS and NLOS conditions, different block lengths, equalizer algorithms and Doppler conditions. All the relevant simulation parameters are given in Table 1. In this table, we use the delay and Doppler resolutions to discretize the channel onto grids. Based on the maximum movement speed and path delay, the maximum Doppler index $k_{v_{max}} = K/2$ and delay order $l_{d_{max}} = L - 1$ are obtained. We also assume that the channel is perfectly known at the receiver and the data bits to be transmitted are uncoded.

From the simulation results, we notice that the BER performance is similar in NLOS channels TDL-A to C or LOS channels TDL-D and E, respectively. In the following performance comparison, we choose TDL-A to represent NLOS and TDL-D to represent LOS channels. Firstly, we compare the BER performance in UMa fast fading channel, assuming a maximum speed of 500 km/h.

TABLE I
Simulation Parameters

Carrier Frequency (f_c)	Subcarrier Spacing (Δf)	No. of Subcarriers (M)	No. of OFDM Symbols (N)
6 GHz	30 KHz	256	32
Bandwidth ($W = M\Delta f$)	Delay Resolution ($d_r = 1/W$)	Duration of OFDM Symbol ($T = M/W$)	Doppler Resolution ($f_r = 1/NT$)
7.68 MHz	130 ns	33333 ns	937.5 Hz
Maximum Speed (v_{max})	Doppler Spread ($f_d = f_c \frac{v_{max}}{v_c}$)	$k_{v_{max}}$ ($\frac{f_d}{f_r}$)	$l_{d_{max}}$ ($\frac{d_{max}}{d_r}$)
500 Km/h	2777.8 Hz	≈ 3	≈ 27

Fig. 3 shows that OTFS performs better than other modulations significantly in fast fading NLOS channels. OFDM and SC-FDMA with M data symbols perform worse because they only explore the frequency diversity. If we extend the number of symbols to $M \times N$, the BER performance of OFDM and SC-FDMA improves notably. For M-point OFDM, we can only use equalization in short segments where slow fading channel is assumed. After extending the signal length with more data symbols, the equalization can exploit time diversity so that the performance is much better.

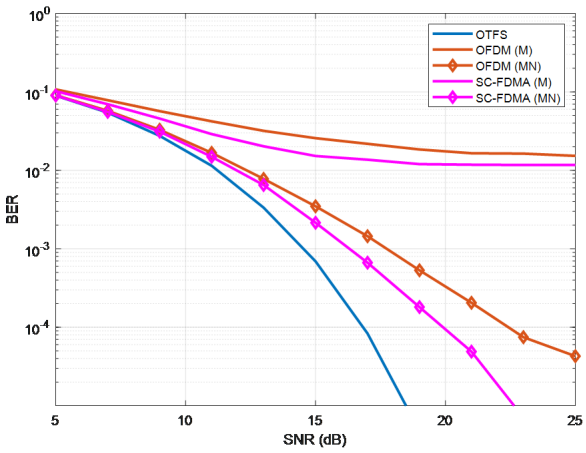

Fig. 3. Performance comparison in fast fading NLOS channels.

In Fig. 4, we compare the BER performance of different modulations in fast fading LOS channels, assuming a maximum speed of 500 km/h. It is shown that the performance of OFDM and SC-FDMA is much closer to OTFS, with only 2 to 3 dB loss.

In Fig. 5 and Fig. 6, we compare the BER performance of different modulations in slow fading NLOS and LOS channels respectively, assuming there is no Doppler effect in

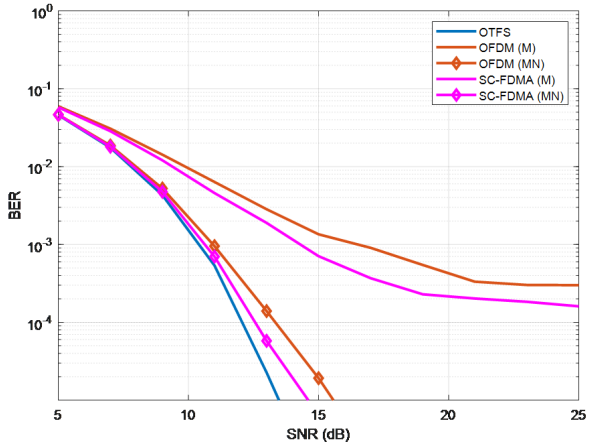

Fig. 4. Performance comparison in fast fading LOS channels.

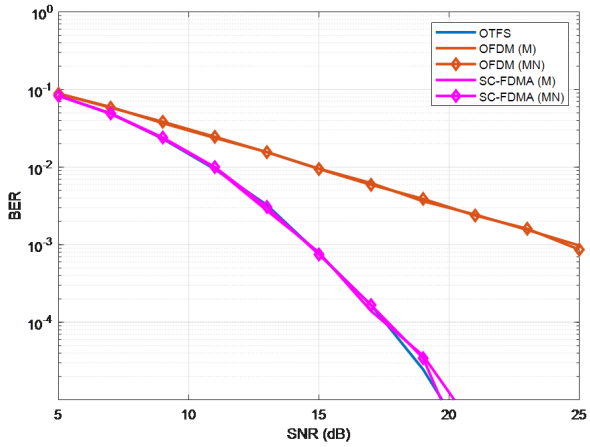

Fig. 5. Performance comparison in slow fading NLOS channels.

the channels. Applying the same MMSE equalization, OTFS performs the same as SC-FDMA with either $M \times N$ or M data symbols.

Fig. 7 shows how OTFS and OFDM perform in UMi Street-canyon, UMa, RMa and UMa O2I channels with Doppler effects. Here, we choose TDL-A as the representative for NLOS channel. The results show that the BERs are similar in all scenarios. For different scenarios, only the delay spread is different. From [15], as the value of M is much larger than L, OTFS and OFDM can both explore the full diversity in the delay domain. Therefore the change of delay spread will not affect the BER performance of these two modulations.

We also compare the performance in TDL-A, B, C, D and E channels under the scenario of UMa. Fig. 8 shows the results in different channels under the same UMa scenario. It is obvious that the performance is similar in LOS or NLOS channel respectively, which proves that we can use TDL-A and TDL-D to represent NLOS and LOS channels respectively.

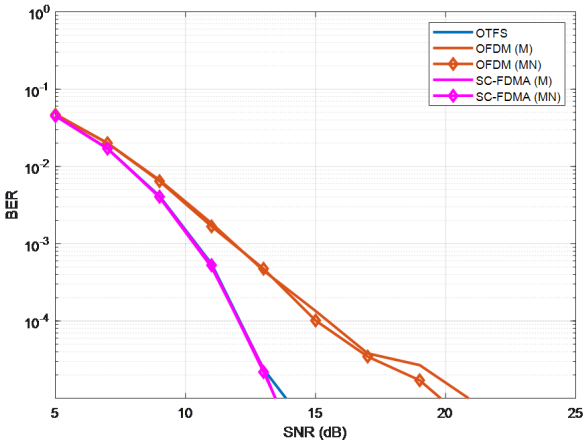

Fig. 6. Performance comparison in slow fading LOS channels.

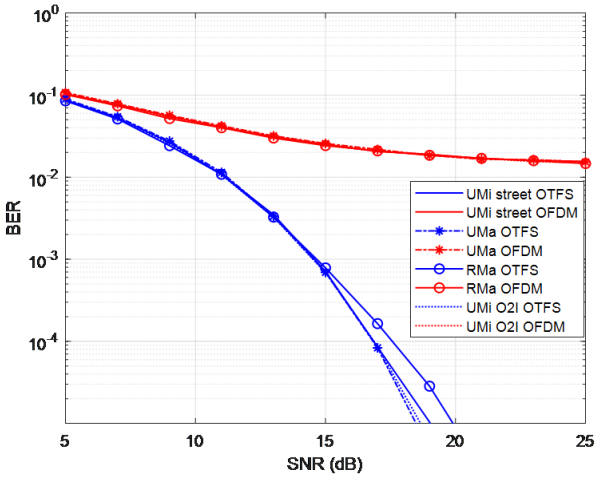

Fig. 7. Performance comparison in different scenarios.

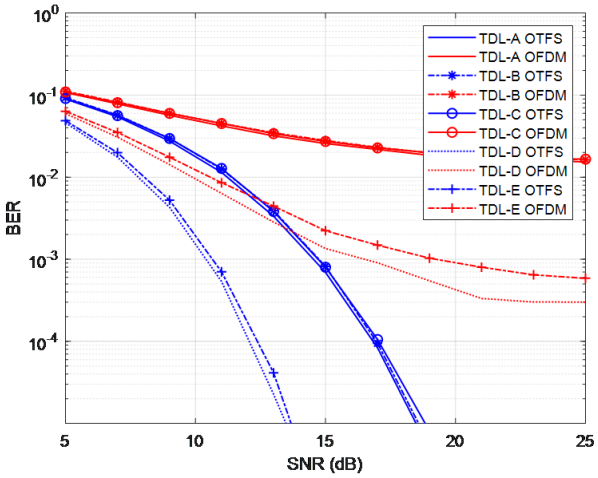

Fig. 8. Performance comparison in different TDL channels.

V. Conclusions

In this paper, we have derived the input and output relationship of OTFS signal in delay-Doppler channels based on the channel delay-time response. From the received OTFS signal expression in matrix form, we have shown that OTFS demonstrates the characteristics of both OFDM and SC-FDMA. Furthermore, we have demonstrated that OTFS can achieve full diversity in both time and frequency domains with the diversity order equaling a product of the number of Doppler shifts and the number of multipaths. Using various TDL channel models, we have conducted BER performance simulation and comparison considering both LOS and NLOS channels. Since OTFS can explore full diversity, the results show that OTFS performs better than other modulations in both fast fading and slow fading channels. The performance gaps between OTFS and others are larger in NLOS channels than those in LOS channels.

Acknowledgment

This research is supported in part by NBN Co under research project PRO18-6384.

References

[1] R. Hadani *et al.*, "Orthogonal time frequency space modulation," in *2017 IEEE Wireless Communications and Networking Conference (WCNC)*, March 2017, pp. 1–6.

[2] F. Wiffen *et al.*, "Comparison of OTFS and OFDM in ray launched sub-6 GHz and mmWave line-of-sight mobility channels," in *2018 IEEE 29th Annual International Symposium on Personal, Indoor and Mobile Radio Communications (PIMRC)*, Sep. 2018, pp. 73–79.

[3] A. Farhang, A. RezazadehReyhani, L. E. Doyle, and B. Farhang-Boroujeny, "Low complexity modem structure for OFDM-based orthogonal time frequency space modulation," *IEEE Wireless Communications Letters*, vol. 7, no. 3, pp. 344–347, June 2018.

[4] A. RezazadehReyhani *et al.*, "Analysis of discrete-time MIMO OFDM-based orthogonal time frequency space modulation," in *2018 IEEE International Conference on Communications (ICC)*, May 2018, pp. 1–6.

[5] P. Raviteja, Y. Hong, E. Viterbo, and E. Biglieri, "Practical pulse-shaping waveforms for reduced-cyclic-prefix OTFS," *IEEE Transactions on Vehicular Technology*, vol. 68, no. 1, pp. 957–961, Jan 2019.

[6] T. Zemen, M. Hofer, D. Löschenbrand, and C. Pacher, "Iterative detection for orthogonal precoding in doubly selective channels," in *2018 IEEE 29th Annual International Symposium on Personal, Indoor and Mobile Radio Communications (PIMRC)*, Sep. 2018, pp. 1–7.

[7] V. Khammammetti and S. K. Mohammed, "OTFS based multiple-access in high Doppler and delay spread wireless channels," *IEEE Wireless Communications Letters*, pp. 1–1, 2018.

[8] K. R. Murali and A. Chockalingam, "On OTFS modulation for high-Doppler fading channels," in *2018 Information Theory and Applications Workshop (ITA)*, Feb 2018, pp. 1–10.

[9] P. Raviteja *et al.*, "Low-complexity iterative detection for orthogonal time frequency space modulation," in *2018 IEEE Wireless Communications and Networking Conference (WCNC)*, April 2018, pp. 1–6.

[10] P. Raviteja, K. T. Phan, Y. Hong, and E. Viterbo, "Interference cancellation and iterative detection for orthogonal time frequency space modulation," *IEEE Transactions on Wireless Communications*, vol. 17, no. 10, pp. 6501–6515, Oct 2018.

[11] P. Raviteja, E. Viterbo, and Y. Hong, "OTFS performance on static multipath channels," *IEEE Wireless Communications Letters*, pp. 1–1, 2019.

[12] M. Kollengode Ramachandran and A. Chockalingam, "MIMO-OTFS in high-Doppler fading channels: Signal detection and channel estimation," in *2018 IEEE Global Communications Conference (GLOBECOM)*, Dec 2018, pp. 206–212.

[13] ETSI, "Study on channel model for frequencies from 0.5 to 100 GHz," *ETSI TR 138 901 V15.0.0*, July 2018.

[14] R. Hadani *et al.*, "Orthogonal time frequency space (OTFS) modulation for millimeter-wave communications systems," in *2017 IEEE MTT-S International Microwave Symposium (IMS)*, June 2017, pp. 681–683.

[15] A. Tajer and A. Nosratinia, "Diversity order in ISI channels with single-carrier frequency-domain equalizers," *IEEE Transactions on Wireless Communications*, vol. 9, no. 3, pp. 1022–1032, March 2010.